Journal of Power Sources 260 (2014) 251–258

Contents lists available at ScienceDirect

Journal of Power Sources

journal homepage: www.elsevier.com/locate/jpowsour

Laser-perforated carbon paper electrodes for improved mass-transport in high power density vanadium redox flow batteries

I. Mayrhuber [a,b,1], C.R. Dennison [a,1], V. Kalra [b,2], E.C. Kumbur [a,*]

[a] Electrochemical Energy Systems Laboratory, Department of Mechanical Engineering and Mechanics, Drexel University, 3141 Chestnut St., Philadelphia, PA 19104, USA
[b] Department of Chemical and Biological Engineering, Drexel University, 3141 Chestnut St., Philadelphia, PA 19104, USA

HIGHLIGHTS

- Laser-perforated carbon paper electrodes are tested in vanadium flow batteries.
- Effects of perforation size, spatial density, and flow rate are investigated.
- Power density of perforated electrodes is improved (30%) compared to raw electrodes.
- Performance improvement is attributed to the enhanced electrolyte accessibility.

ARTICLE INFO

Article history:
Received 11 December 2013
Received in revised form
28 January 2014
Accepted 5 March 2014
Available online 18 March 2014

Keywords:
Electrode
Performance
Power density
Transport
Vanadium flow battery

ABSTRACT

In this study, we demonstrate up to 30% increase in power density of carbon paper electrodes for vanadium redox flow batteries (VRFB) by introducing perforations into the structure of electrodes. A CO_2 laser was used to generate holes ranging from 171 to 421 μm diameter, and hole densities from 96.8 to 649.8 holes cm^{-2}. Perforation of the carbon paper electrodes was observed to improve cell performance in the activation region due to thermal treatment of the area around the perforations. Results also demonstrate improved mass transport, resulting in enhanced peak power and limiting current density. However, excessive perforation of the electrode yielded a decrease in performance due to reduced available surface area. A 30% increase in peak power density (478 mW cm^{-2}) was observed for the laser perforated electrode with 234 μm diameter holes and 352.8 holes cm^{-2} (1764 holes per 5 cm^2 electrode), despite a 15% decrease in total surface area compared to the raw un-perforated electrode. Additionally, the effect of perforation on VRFB performance was studied at different flow rates (up to 120 mL min^{-1}) for the optimized electrode architecture. A maximum power density of 543 mW cm^{-2} was achieved at 120 mL min^{-1}.

1. Introduction

Redox flow batteries (RFBs) are emerging as a promising energy storage technology for a broad range of applications. These batteries can be used as medium- to large-scale energy storage systems, which are implemented into the electrical grid to store or deliver energy based on demand. Furthermore, this technology can be used for emergency back-up applications to replace diesel generators as uninterruptible power supplies (UPS), or as a stand-alone device to store and deliver electric power in remote areas and micro-grids [1–3]. The key advantage of flow battery systems is that their energy capacity and power output are decoupled, unlike conventional secondary batteries. Accordingly, the energy capacity of a RFB is determined by the size of the electrolyte reservoirs, while the power output is determined by the electrochemical cell stack (size and number of cells) [1–3]. Other advantages of this technology are fairly long cycle-lifetimes, and the ability to deep-discharge the system without adversely affecting its lifetime. Additionally, the need for cell balancing is eliminated, unlike other secondary battery technologies, because all cells in the stack are supplied from the same storage tanks. Many redox chemistries can be applied in

* Corresponding author. Tel.: +1 215 895 5871; fax: +1 215 895 1478.
E-mail addresses: vk99@drexel.edu (V. Kalra), eck32@drexel.edu (E.C. Kumbur).
[1] Equal contribution.
[2] Tel.: +1 215 895 2233; fax: +1 215 895 5837.

http://dx.doi.org/10.1016/j.jpowsour.2014.03.007
0378-7753/

RFB systems, however the 'all-vanadium' chemistry is among the most extensively studied [1–4] due to the advantages of using the same, but differently charged, active species in both half cells.

Although vanadium redox flow batteries (VRFBs) offer a number of advantages, there are several limitations which hinder their widespread implementation. One disadvantage is the relatively low energy density (40 Wh L^{-1}) [1–3]. Although low energy density is a significant problem for transportation applications, it is not necessarily a major issue for stationary use of a VRFB system, where mass and volume constraints are much less important. Similarly, the power density of a VRFB cell is relatively low compared to lead-acid and lithium-ion batteries. As a result, larger cells must be used to satisfy the power demand, leading to a significant increase in cost. Therefore, any appreciable improvements in power density can yield significant cost-savings, making VRFBs more competitive for grid-scale applications.

The power generated by a VRFB is primarily governed by the electrodes. The electrodes in a VRFB are responsible for hosting the redox reactions and for facilitating the transport of both electrons (through the solid phase) and chemical reactants (through the pore phase) to the reaction sites. Thus, the major factors limiting the power density of a VRFB are kinetic, ohmic, and mass transport losses associated with the electrodes [2,3]. These factors are primarily determined by surface functionality, electronic resistance, cell architecture and pore structure of the electrode material.

Recently, significant work has been done to improve the electrodes of the VRFB systems in order to increase power density and lower system cost [5–18]. The main emphasis in these studies has been placed on improving the surface area, surface chemistry, pore size distribution and conductivity of the material to improve the reaction kinetics and mass transport ability and reduce the areal series resistance (ASR). Until recently, carbon felts were the most commonly employed electrode materials in VRFBs [6]. Although no catalyst is necessary to facilitate the redox reactions, reaction kinetics still play an important role on system performance, and much work has been done to understand and improve the surface chemistry of carbon felts [6–11]. To-date, thermal treatments, similar to those described by Sun et al. [9], are considered to be the most common practice employed to functionalize carbon felt electrodes and improve their electrochemical performance.

Beyond kinetics, the effective delivery and removal of reactants is another important consideration, which has not been thoroughly studied. Qiu et al. performed pore-scale simulations utilizing XCT-reconstructed electrode morphologies to predict cell performance and localized phenomena inside carbon felt electrodes [12,13]. The authors investigated electrodes with porosities ranging from 84.5% to 93.2% and observed lower localized current density and overpotential fields with increased pressure drop for the lower porosity electrodes. Under normal operating conditions, however, the performance of the simulated carbon felt electrodes was not found to be limited by mass transport losses.

Recently, Mench and co-workers utilized carbon paper as an electrode material for VRFBs [14–16]. These materials are 5×–10× thinner than carbon felts which enables reduced transport pathlengths for both electrons and ions, resulting in reduced ASR. Moreover, the porosity and pore-size of this material are reduced compared to carbon felt, giving rise to increased specific surface area and thus a higher limiting current density. In a recent study, they demonstrated a VRFB with a peak power of 557 mW cm^{-2}, which is significantly higher than what had previously been reported in literature [14]. They accomplished this by stacking sheets of carbon paper as the electrodes in each half cell. Additionally, they varied the number of sheets stacked in each half cell in order to study the tradeoff between resistance and surface area. They identified an optimal stack height of three sheets of carbon paper per half-cell, corresponding to an uncompressed thickness of 1230 μm per electrode [14].

Manahan et al. expanded on this work by modifying carbon paper electrodes with a thin layer of multi-walled carbon nanotubes (CNTs), and then testing the performance of a VRFB with the CNT-treated layer facing either the membrane or flow field side in both half-cells [15]. Experiments showed that cell voltage and power density improved the most when the CNT layer faced the current collector, especially at the negative side. Based on these findings, they pointed out three important observations: a) the majority of the reactions happen near the current collector, b) CNTs improved electrical contact with the current collectors, and c) the negative electrode is the rate-limiting electrode [14], in agreement with other studies [5].

Liu et al. further improved the performance of a vanadium flow battery using a no-gap architecture by thermal pre-treatment of the carbon paper electrodes in argon and air [16]. The air treatment showed a greater power density improvement (16% compared to raw material) than argon treatment. This result was attributed to an increase in oxygen containing functional groups, which improved the reaction kinetics at the electrode surface. By optimizing the surface area/chemistry, conductivity of the electrodes, and changing the membrane material, the authors demonstrated a power density of 767 mW cm^{-2}, which is the highest power density reported to-date [16].

As these studies show, the most common approach to improving the power density of VRFBs is by increasing the available surface area, decreasing ohmic resistance, and maximizing reaction kinetics. Although significant progress has been achieved through the use of functionalized, high surface area carbon paper electrodes, further improvement of the power density is still necessary to further reduce the cost of these systems. A major aspect of electrode design which has been largely ignored in previous studies is the capability of the electrode to quickly deliver fresh reactant to the available reaction sites. Although the effect of electrode microstructure has previously been explored using numerical simulations [12,13], these simulations were applied primarily to carbon felt materials with very high porosity, and relatively large pores. Here, we hypothesize that mass transport is a limiting factor for more dense, high-power carbon paper electrodes, and by improving the accessibility to the available active surface area it is possible to further increase the power density of existing electrode materials.

Motivated by this hypothesis, our goal in this study was to better understand the mass transport limitations associated with high power density carbon paper electrodes, and to identify mitigation strategies which improve the electrolyte accessibility and further enhance power density of these materials. Specifically, we investigated the effects of macro-scale perforations ("transport channels"), on the power density and performance of the carbon paper electrodes in a VRFB system. These transport channels are expected to provide a more facile route for electrolyte to enter and permeate through the electrode, thus improving the supply of reactants to the active surface area of the material. Our approach is similar to that reported in a study by Manahan et al., where they perforated 300 μm diameter holes into the micro-porous layer of a polymer electrolyte fuel cell to improve the transport of liquid water through the cell [19,20]. Here, we used a CO_2 laser to open transport pathways of varying size and number in the electrode structure. By varying the diameter and density of these transport channels, we studied the effects of perforation size and the critical transport length for electrolyte flowing through the bulk electrode material. Additionally, the flow rate in the cell was varied to better understand the effect of these perforations (i.e., transport channels) under different mass transport conditions.

2. Method of approach

2.1. VRFB cell

The VRFB used in this study was composed of a single cell with two graphite current collector plates, each with a serpentine flow field (Fuel Cell Technologies). Carbon paper electrodes (10AA carbon paper from SGL Carbon Group, Germany) with 410 μm nominal thickness and 5 cm^2 active area were used in this study. In each half-cell, 3 sheets of electrodes were stacked, leading to a total nominal electrode thickness of 1230 μm per side. This electrode configuration was chosen because it demonstrated optimum power density in Ref. [14]. Viton rubber gaskets (DuPont, thickness 0.8 mm) were used between the components to prevent electrolyte leakage and to limit the compression of the electrode to ~35% in order to reduce contact resistance within the cell. Nafion 117 (Dupont) was used as the ion exchange membrane to separate the half-cells. The cell was connected to the electrolyte tanks using Tygon tubing (Saint-Gobain), and two peristaltic pumps (Cole Parmer) supplied electrolyte to the cell at a constant flow rate of 20 mL min^{-1} (unless otherwise stated).

2.2. Electrolyte preparation

The all-vanadium electrolyte was synthesized by dissolving vanadium (IV) oxide sulfate hydrate ($VOSO_4 \cdot xH_2O$, Sigma Aldrich) in a solution of sulfuric acid and deionized (DI) water. The final concentrations were 1 M vanadium and 5 M SO_4^{2-}. From this starting solution, electrolyte in the fully charged state for the positive and negative half-cells (V(V) and (VII), respectively) were prepared using the electrochemical method described in Ref. [5]. During all tests, the electrolyte volumes in each negative and positive tank were 50 mL. The electrolyte tanks maintained a continuous nitrogen blanket above the electrolytes, and were purged with nitrogen prior to start of measurements in order to prevent oxidation of the vanadium species.

2.3. Electrochemical measurements

All performance measurements were performed using a Scribner Associates 857 Redox Flow Cell Test System. Polarization curves were recorded by applying a series of galvanostatic discharge steps, starting from ~100% state-of-charge (SoC). The current steps were evenly spaced using 100 mA increments (20 mA cm^{-2}) and lasted 30 s each to allow the system to stabilize. Discharge was terminated when the cell voltage dropped below 0.2 V. The charged state of the cell (~100% SoC) was assumed to be reached after the charging current dropped below 10 mA (2 mA cm^{-2}) while applying a constant potential of 1.8 V to the cell. During all tests, the high-frequency resistance (HFR) was measured at a frequency of 10 kHz. The areal specific resistance (ASR) was calculated by multiplying the HFR and the electrode area (5 cm^2).

2.4. Laser-perforation

In order to determine the effects of laser perforation on electrode performance, 8 different perforation (also referred to simply as 'holes', for brevity) patterns were designed (see Fig. 1). Cases 1 through 4 had a constant hole density of 900 holes per 5 cm^2 electrode (180 holes cm^{-2}) with hole diameters varying from 171 to 421 μm. Cases 5 through 8 had a nominal hole diameter of 234 μm and a hole density ranging from 484 to 3249 holes per 5 cm^2 electrode (96.8–649.8 holes cm^{-2}). These configurations were selected to study the effects of hole diameter (Cases 1 through 4) and hole density (Cases 5 through 8) on the system performance. A schematic and summary of all Cases tested are provided in Fig. 1.

For each case, the perforations were made in a Cartesian grid-pattern (Fig. 1). For this reason, the total number of holes per 5 cm^2 electrode was constrained to square numbers (e.g., 484 holes per 5 cm^2 electrode corresponds to a 22×22 grid). As a raw electrode material, non-perforated SGL 10AA carbon paper was chosen because it has the highest reported power density to-date [16]. Raw SGL 10AA was characterized and considered as the baseline case to compare the laser-perforated electrodes against. In all cases, the material was used as-received, without any form of pre-treatment.

Perforation of the raw material was performed using an EPILOG mini 45 W CO_2 laser cutting machine. During cutting, a sheet of carbon paper was fixed to a graphite backing plate with tape in order to ensure a flat surface during cutting, and thus a well-focused laser beam. The cutting process was performed twice to ensure that the laser penetrated the material completely and a clean cut without residues was achieved. The laser perforation process was quite rapid: more than 50,000 individual perforations could be produced approximately 1.5 h, which is equivalent 20 or

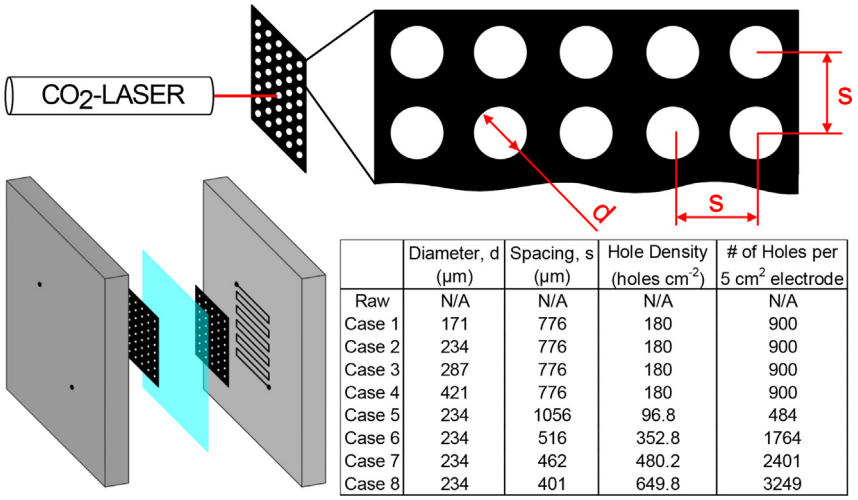

	Diameter, d (μm)	Spacing, s (μm)	Hole Density (holes cm^{-2})	# of Holes per 5 cm^2 electrode
Raw	N/A	N/A	N/A	N/A
Case 1	171	776	180	900
Case 2	234	776	180	900
Case 3	287	776	180	900
Case 4	421	776	180	900
Case 5	234	1056	96.8	484
Case 6	234	516	352.8	1764
Case 7	234	462	480.2	2401
Case 8	234	401	649.8	3249

Fig. 1. Schematic of the flow cell setup with laser-perforated electrodes and the laser perforation process. The table summarizes all the cases studied that have different electrode configuration (i.e., different hole diameter and number of holes).

more of the electrodes used in this study (depending on the complexity of the pattern). Fairly conservative laser cutting parameters (e.g. laser power, vector speed, etc.) were used to manufacture the electrodes in this study. In practice, the cutting time could be significantly reduced by using a higher powered laser and optimizing the cutting parameters.

Fig. 2 shows a typical hole at each selected diameter value. The images were taken with a Carl Zeiss Supra 55 scanning electron microscope (SEM). All diameter values used in this study are an average of spatial measurements determined from the SEM micrographs. The observed holes are not perfectly circular in shape. This is likely due to the limited spatial resolution of the laser cutting machine, errors in beam focusing, and the varying density of the carbon paper. The standard deviation observed at each hole diameter is 18, 32, 47, and 25 μm for electrodes with nominal diameters of 171, 234, 287, and 421 μm, respectively.

Fig. 3 shows the spacing between the laser-perforated holes for varying hole densities (number of holes per electrode). The spacing measurements were performed using a Nikon ECLIPSE ME600 microscope, and the images shown were taken on a Nikon SMZ800 stereo microscope. The spacing between holes was found to be quite uniform for all samples examined.

3. Results and discussion

3.1. Role of perforation size on VRFB performance

The first set of laser perforated electrodes tested (Cases 1–4) had hole sizes ranging from 171 to 421 μm in diameter at a constant hole density of 180 holes cm^{-2} (900 holes per 5 cm^2 electrode). In order to determine the effect of perforation diameter, polarization curves for each electrode were recorded at a flow rate of 20 mL min^{-1}. The polarization curves are shown in Fig. 4a, and the peak power density and limiting current density extracted from these plots are shown in Fig. 4b. Additionally, the primary measures of performance for each case are summarized in Table 1.

From the results (Fig. 4a), it is observed that the laser-perforated electrodes exhibit increased average voltage and power density compared to the raw material. The electrode with 234 μm hole diameter shows the highest peak power density of 447 mW cm^{-2}, while the electrodes with smaller and larger diameter holes exhibit slightly lower peak power densities (Fig. 4b). In comparison to this, the raw electrode shows a much lower peak power density of only 369 mW cm^{-2}. All electrodes tested show a consistent ASR around 0.6 Ω cm^2, which is comparable to previously reported results for carbon paper electrodes [14–16].

When the polarization curves for the laser-perforated electrodes (Fig. 4a) are analyzed, an improvement in the kinetic region of the polarization curve (~0–100 mA cm^{-2}) is observed, which scales with increasing hole diameter. This improvement is likely due to the local surface functionalization of the material surrounding each hole. Manahan et al. [19,20] showed the presence of a 'heat affected zone' (HAZ) around laser-perforations in a similar carbon paper material (SGL 10BB) commonly used in PEM fuel cell applications. This HAZ was observed to extend ~200 μm radially from the center of the hole. It was reported that PTFE (found in the virgin electrode material used in the study) was largely removed in the HAZ, indicating that the area reached a temperature sufficient to decompose PTFE (>350 °C). Liu et al. have demonstrated that SGL 10AA carbon paper can be thermally treated at similar temperatures (400 °C) in an air atmosphere, providing a noticeable improvement in peak power and limiting current density. Based on these previous observations, it is plausible that the material surrounding the perforations in the present study was effectively 'thermally treated' during laser perforation in a similar manner to Liu et al. [16], giving rise to the observed improvement in the kinetic region.

In addition to the improved performance in the activation region, the observed improvements in limiting current and power density are also attributed to increased accessibility of active surface area in the perforated electrodes. In Fig. 4a, this is indicated by the delayed downward deflection of the polarization curve at higher current densities, indicating improved mass transport in the electrodes. It is interesting to note that the limiting current density (Fig. 4b) is significantly increased for the perforated electrodes with hole diameters up to 287 μm, even though the total active surface area of these electrodes is decreased by 4% (for hole diameter ø = 171 μm), 8% (ø = 234 μm) and 12% (ø = 287 μm) due to laser-perforation. However, although the electrode with the largest perforations (ø = 421 μm) shows a very respectable power density of 440 mW cm^{-2} at low current densities (<500 mA cm^{-2}), a rapid

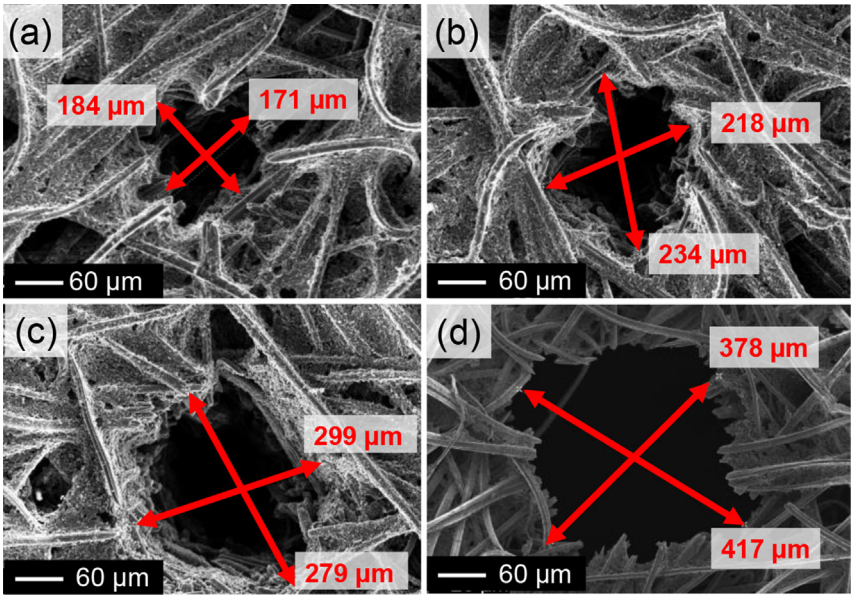

Fig. 2. SEM images of laser-perforated holes in carbon paper electrodes with an average of hole diameter of (a) 171 μm, (b) 234 μm, (c) 287 μm and (d) 421 μm.

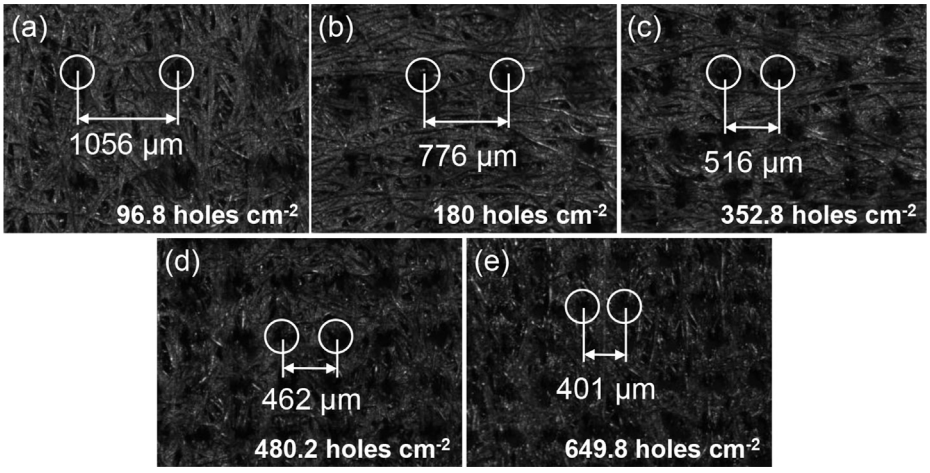

Fig. 3. Spacing between holes for different hole densities: (a) 96.8, (b) 180, (c) 352.8, (d) 480.2 and (e) 649.8 holes cm^{-2}.

decrease in voltage occurs above 500 mA cm^{-2}, resulting in a limiting current similar to the raw electrode. These results suggest a tradeoff between mass transport and available surface area in these carbon paper electrodes. The apparent peak in limiting current between 171 and 234 µm hole diameter observed in Fig. 4b indicates a substantial mass-transport limitation in the raw material. When the data is compared for different electrode configurations, the introduction of laser-perforations seems to improve the ability of the electrolyte to access the available surface area in the electrodes, leading to an increase in the limiting current density. However, laser perforation removes a portion of the available surface area (Table 1). As the perforations increase in diameter, electrolyte accessibility appears to be improved at the expense of available surface area. Therefore, the electrode with the largest perforations ($ø = 421$ µm) is likely limited by the total surface area remaining after perforation, rather than the electrolyte accessibility.

3.2. Role of perforation density on VRFB performance

A second set of electrodes (Cases 2, 5–8) with a varying density (number) of holes ranging from 484 to 3249 holes per 5 cm^2 electrode (96.8–649.8 holes cm^{-2}) were tested to investigate the effect of hole density on device performance. Although the specific number of holes were specified for each electrode in this study, hole density (holes cm^{-2}) is used here as a reference parameter to provide a normalized value, which can be extended to systems of varying size. Changing the hole density not only affects the total number of transport channels available for mass transport, it also affects the distance that electrolyte must travel into the bulk of the electrode. The hole spacing (center-to-center) is provided as an indicator of the distance that electrolyte has to travel between holes (see Table 2). As the spacing between holes decreases, mass transport is expected to improve because electrolyte does not need to travel as far to fully access the available surface area. Based on the previous tests, a hole diameter of 234 µm was chosen as the standard hole size for these Cases, as this diameter was observed to provide the highest power density of the hole sizes tested (see Fig. 4b). The results of these tests are shown in Fig. 5.

As in the previous test series, all of the laser-perforated electrodes demonstrate improved performance in the activation region of the polarization curve (Fig. 5a). As stated earlier, this is believed to be caused by the localized thermal treatment of the fibers directly surrounding the holes due to heat generated during the

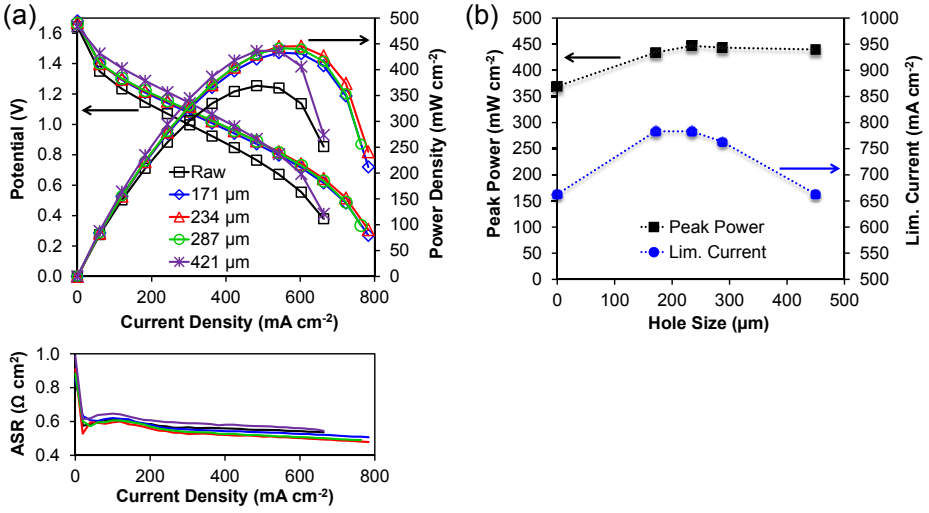

Fig. 4. (a) Polarization curves and measured ASR for perforated electrodes with varying hole size, and (b) extracted peak power and limiting current density values at a constant flow rate of 20 mL min^{-1}.

Table 1
Performance metrics for electrodes with various diameter laser perforations at a constant hole density of 180 holes cm^{-2}.

Case number	Hole diameter (μm)	OCV (V)	Area specific resistance (mΩ cm^2)	Limiting current density at 20 mL min^{-1} flow rate (mA cm^{-2})	Peak power density (mW cm^{-2})	Change in surface area vs. raw (%)	Approx. porosity (%)
Raw	N/A	1.64	537–615	663	369	0	88
1	171	1.68	507–633	783	434	−4	84
2	234	1.67	479–600	783	447	−8	81
3	287	1.66	490–606	763	443	−12	78
4	421	1.64	545–647	663	440	−25	66

laser perforation. However, only the electrodes with 180 and 352.8 holes cm^{-2} (i.e., 900 and 1764 holes per 5 cm^2 electrode, respectively) exhibit a substantial improvement in the mass-transport region (i.e., high current densities). As seen in Fig. 5b, the limiting current for these intermediate hole-density electrodes is observed to be significantly higher than the other cases tested, indicating a good balance of electrolyte accessibility and surface area remaining after perforation. On the other hand, the electrode with the fewest perforations (i.e., 96.8 holes cm^{-2}–484 holes per 5 cm^2 electrode) is still likely limited by the ability of the electrolyte to access to all of the available surface area. Conversely, the electrodes with the most perforations (i.e., 480.2 and 649.8 holes cm^{-2}–2401 and 3249 holes per 5 cm^2 electrode, respectively) appear to be limited by the remaining electrode surface area, rather than electrolyte accessibility.

In terms of power density, as the hole density was increased from 96.8 to 352.8 holes cm^{-2} (484–1764 holes per 5 cm^2 electrode, respectively), the power density was found to increase to a maximum of 478 mW cm^{-2}, compared to 369 mW cm^{-2} for the raw electrode (Fig. 5b). For the case with 352.8 holes cm^{-2}, this corresponds to an increase in peak power of 30% versus the raw electrode. However, beyond 352.8 holes cm^{-2}, the creation of additional perforations was seen to decrease the power density. In fact, the performance of electrode with 649.8 holes cm^{-2} (3249 holes per 5 cm^2 electrode) falls below the peak power density and limiting current of the raw electrode. Similar to the hole diameter study, the reason for this decrease is believed to be the excessive amount of surface area lost due to perforation.

Additionally, the electrode with 649.8 holes cm^{-2} (3249 holes per 5 cm^2 electrode) was observed to be visibly thinner and more flexible than all other electrodes tested. The large amount of material removed during laser-perforation (~28% material loss) is believed to have decreased the stability of the carbon paper, resulting in a lower compression pressure under normal assembly and greater ASR due to increased contact resistance. While the average ASR for most of the electrodes studied was below 0.6 Ω cm^2, the ASR for the electrode with 649.8 holes cm^{-2} was observed to be significantly higher (~0.8 Ω cm^2).

3.3. Role of flow rate on the performance of perforated electrodes

In order to better understand the role of perforations on mass transport within the electrode, the effect of flow rate was also investigated. Based on the previous results, the best-performing electrode at a flow rate of 20 mL min^{-1} was found to be Case 6 (ø = 234 μm and 352.8 holes cm^{-2}). Polarization curves for this electrode were conducted at flow rates of 40, 60, 90 and 120 mL min^{-1} to further highlight the benefits of laser perforations for improving mass transport in the cell. The results are shown in Fig. 6.

As shown in Fig. 6, all tested cases follow the same trend below 500 mA cm^{-2}. At 20 mL min^{-1}, the onset of mass transport limitations appears to begin around 500 mA cm^{-2}, whereas for the other flow rates tested, the mass transport limitation appears to start around 625–650 mA cm^{-2}. When the overall trend is analyzed, the mass transport losses seem to be reduced with increasing flow rate for the tested perforated electrode. As expected, higher flow rates lead to incremental improvements in performance at higher current densities, although the difference in performance between 90 and 120 mL min^{-1} is small. The ASR was observed to remain between 0.5 and 0.6 Ω cm^2 for all tests.

Fig. 7 shows the peak power and the limiting current density of our best performing electrode (hole diameter of 234 μm and 352.8 holes cm^{-2}) compared to the raw electrode at various flow rates. For the highest tested flow rate of 120 mL min^{-1}, the peak power for the raw electrode was around 429 mW cm^{-2}, while the perforated electrode exhibited 543 mW cm^{-2} (27% higher than the raw electrode). At a more conventional flow rate of 20 mL min^{-1}, the peak power is observed to increase from 369 mW cm^{-2} for the raw electrode, whereas for the perforated electrode, it goes up to 478 mW cm^{-2} (30% increase). Similarly, the limiting current densities at 20 mL min^{-1} are found to increase from 663 mA cm^{-2} for the raw electrode to 763 mA cm^{-2} for the perforated electrodes (15% increase). At 120 mL min^{-1}, the raw electrode demonstrated 844 mA cm^{-2} while the perforated electrode produced 924 mA cm^{-2} (9% increase). Based on these results, it appears that the effectiveness of the laser perforations is not diminished at higher flow rates. This indicates that mass transport within the raw carbon paper electrodes is consistently limited, even at higher flow rates when more advantageous concentration and pressure gradients are present.

It is worth pointing out that at a flow rate of 90 mL min^{-1}, the raw SGL 10AA electrode was observed to deliver 424 mW cm^{-2}. Under similar conditions, however, Aaron et al. were able to reach a peak power of 557 mW cm^{-2} [14]. The lower absolute power density observed in this study is believed to be due to variations in

Table 2
Performance metrics for electrodes with different number of holes per electrode (i.e., hole density) at a constant hole diameter of 234 μm.

Case number	Hole density (holes cm^{-2})	Hole spacing (μm)	OCV (V)	Area specific resistance (mΩ cm^2)	Limiting current density at 20 mL min^{-1} flow rate (mA cm^{-2})	Peak power density (mW cm^{-2})	Change in surface area vs. raw (%)	Approx. porosity (%)
Raw	N/A	N/A	1.64	537–615	663	369	0	88
5	96.8	1056	1.64	472–561	683	413	−4	84
2	180	776	1.67	479–600	783	447	−8	81
6	352.8	516	1.66	475–578	763	478	−15	75
7	480.2	462	1.63	498–579	643	445	−21	70
8	649.8	401	1.63	703–922	643	364	−28	63

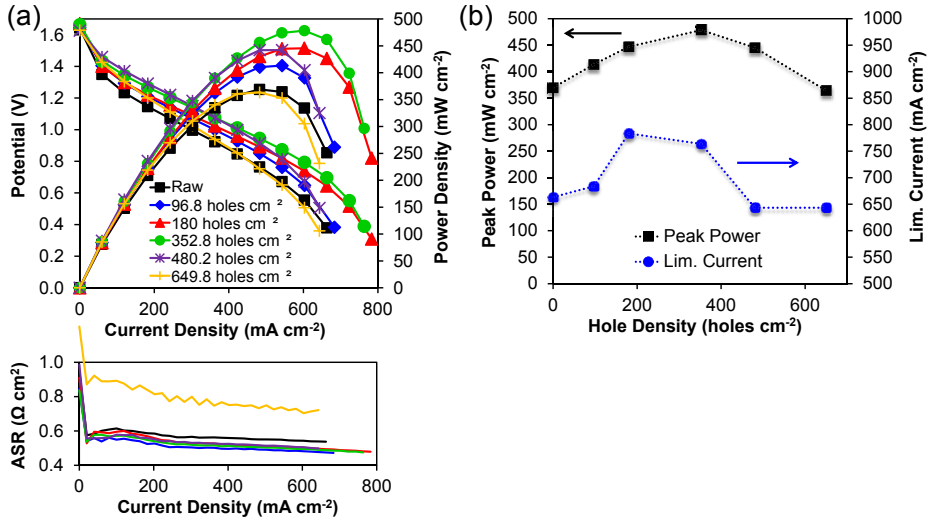

Fig. 5. (a) Polarization curves and measured ASR for perforated electrodes with varying hole density (number of holes), and (b) extracted peak power and limiting current density values at a constant flow rate of 20 mL min^{-1}.

the experimental setup. Nonetheless, similar relative improvements (up to 30%) are expected when implementing these laser perforated electrodes into more optimized cells, leading to even higher absolute power- and limiting current densities than are reported here.

4. Conclusion

In this study, the performance of a VRFB was investigated using raw and laser-perforated SGL 10AA carbon paper electrodes in a zero-gap serpentine flow field cell design. The carbon paper electrodes were laser-perforated in order to create 'transport channels' for improved mass transport within the electrode. The laser perforation process was quite efficient: more than 50,000 individual perforations could be produced approximately 1.5 h, which is equivalent 20 or more of the electrodes used in this study (depending on the complexity of the pattern). In this work, three parameters were studied: hole size (diameter), hole density (number of holes per cm^2), and flow rate. By testing a series of electrodes with different hole diameters and hole densities, a maximum power density of 478 mW cm^{-2} was achieved using an electrode with 234 μm diameter holes at a hole density of 352.8 holes cm^{-2} (1764 holes per 5 cm^2 electrode) and flow rate of 20 mL min^{-1}. This corresponds to a 30% increase in power density compared to the raw, un-perforated material (369 mW cm^{-2}). Similarly, the limiting current for this perforated electrode exhibited a 15% increase (763 mA cm^{-2}) compared to the raw electrode (663 mA cm^{-2}).

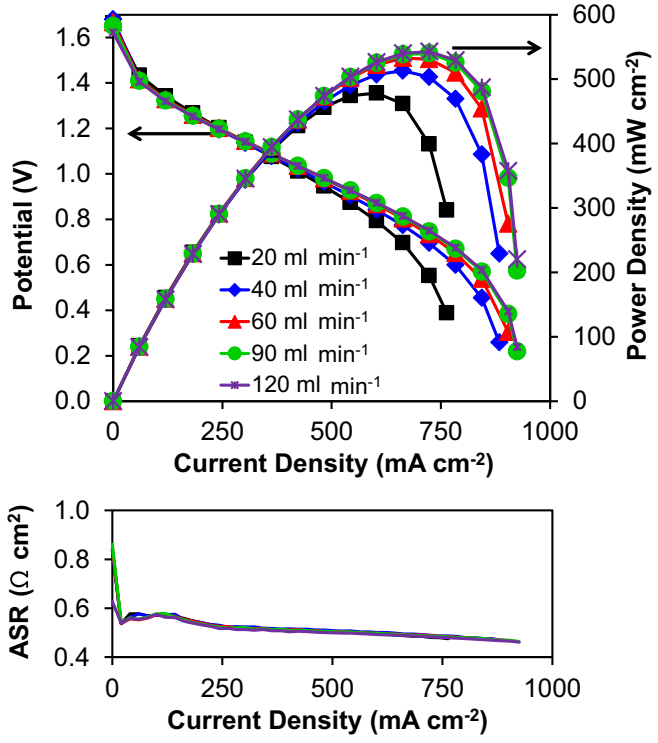

Fig. 6. Polarization curves and corresponding ASR at various flow rates for Case 6 (hole diameter = 234 μm, hole density = 352.8 holes cm^{-2}).

Despite a loss in total surface area, the improved performance of the modified electrode is largely attributed to the increased mass transport ability provided by the laser perforations, which act as pathways for the electrolyte to better penetrate the electrode. However, excessive perforation of the electrode may reduce both power density and limiting current density due to the significant loss of surface area. The laser perforated electrodes were also observed to have better performance in the activation region of the polarization curve. This improvement is believed to be due to the localized heating of the fibers surrounding the holes during perforation, which improves the kinetics of the electrodes.

Additionally, the effect of perforation on battery performance was studied at different flow rates. Results show that the addition of perforations improves power and current density over a wide range of flow rates. At a flow rate of 120 mL min^{-1}, a maximum power density of 543 mW cm^{-2} was achieved. Compared to the raw material (429 mW cm^{-2} at 120 mL min^{-1}), this is an increase of 27%. However, slightly larger improvements (up to 30% at 20 mL min^{-1}) were observed for perforated electrodes at lower flow rates, when the system is more prone to mass transport limitations and these 'transport channels' are even more critical.

Results of this study show that the use of laser-perforated electrodes in an optimized configuration increases the

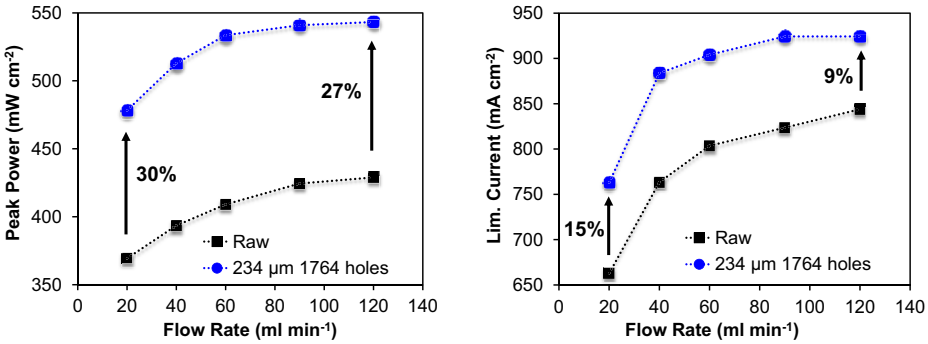

Fig. 7. Peak power and limiting current as a function of the flow rate for the raw electrode and Case 6 (hole diameter = 234 μm, hole density = 352.8 holes cm^{-2}).

performance of a VRFB (up to 30% in this study) compared to raw carbon paper, despite a significant loss in the total active surface area (15% for the highest performing electrode in this study) due to the laser perforations. These findings highlight the fact that by properly tailoring the transport pathways in the electrode structure, it is possible to further enhance the power density of the electrodes used in these systems.

Acknowledgments

The authors wish to thank Jeff Kahn and Professor James Tangorra at Drexel University for their assistance and the use of their laser cutter. The authors also acknowledge Richa Singhal and Ivan Garcia Torregrosa for their assistance with SEM imaging. IM acknowledges the Erasmus Mundus – Materials for Energy Storage and Conversion Master Program. VK acknowledges the support from National Science Foundation (Grant # CBET 1236466).

References

[1] M. Skyllas-Kazacos, M.H. Chakrabarti, S.A. Hajimolana, F.S. Mjalli, M. Saleem, J. Electrochem. Soc. 158 (2011) R55–R79.
[2] A. Parasuraman, T.M. Lim, C. Menictas, M. Skyllas-Kazacos, Electrochim. Acta 101 (2013) 27–40.
[3] N. Trung, R.F. Savinell, Electrochem. Soc. Interface 19 (2010) 54–56.
[4] K.W. Knehr, E. Agar, C.R. Dennison, A.R. Kalidindi, E.C. Kumbur, J. Electrochem. Soc. 159 (2012) A1446–A1459.
[5] E. Agar, C.R. Dennison, K.W. Knehr, E.C. Kumbur, J. Power Sources 225 (2013) 89–94.
[6] S. Zhong, C. Padeste, M. Kazacos, M. Skyllas-Kazacos, J. Power Sources 45 (1993) 29–41.
[7] W.H. Wang, X.D. Wang, Electrochim. Acta 52 (2007) 6755–6762.
[8] Z. Gonzalez, C. Botas, P. Alvarez, S. Roldan, C. Blanco, R. Santamaria, M. Granda, R. Menendez, Carbon 50 (2012) 828–834.
[9] B. Sun, M. Skyllas-Kazacos, Electrochim. Acta 37 (1992) 1253–1260.
[10] B. Sun, M. Skyllas-Kazacos, Electrochim. Acta 37 (1992) 2459–2465.
[11] W. Guanjie, J. Chuankun, L. Jianguo, Y. Chuanwei, J. Power Sources 220 (2012) 185–192.
[12] G. Qiu, A.S. Joshi, C.R. Dennison, K.W. Knehr, E.C. Kumbur, Y. Sun, Electrochim. Acta 64 (2012) 46–64.
[13] G. Qiu, C.R. Dennison, K.W. Knehr, E.C. Kumbur, S. Ying, J. Power Sources 219 (2012) 223–234.
[14] D.S. Aaron, Q. Liu, Z. Tang, G.M. Grim, A.B. Papandrew, A. Turhan, T.A. Zawodzinski, M.M. Mench, J. Power Sources 206 (2012) 450–453.
[15] M.P. Manahan, Q.H. Liu, M.L. Gross, M.M. Mench, J. Power Sources 222 (2013) 498–502.
[16] Q.H. Liu, G.M. Grim, A.B. Papandrew, A. Turhan, T.A. Zawodzinski, M.M. Mench, J. Electrochem. Soc. 159 (2012) 1246–1252.
[17] L. Yue, W. Li, F. Sun, L. Zhao, L. Xing, Carbon 48 (2010) 3079–3090.
[18] C.-N. Sun, F.M. Delnick, D.S. Aaron, A.B. Papandrew, M.M. Mench, T.A. Zawodzinski, ECS Electrochem. Lett. 2 (2013) A43–A45.
[19] M.P. Manahan, M.C. Hatzell, E.C. Kumbur, M.M. Mench, J. Power Sources 196 (2011) 5573–5582.
[20] M.P. Manahan, M.M. Mench, J. Electrochem. Soc. 159 (2012) F322–F330.